Hindawi Publishing Corporation
EURASIP Journal on Advances in Signal Processing
Volume 2008, Article ID 657081, 8 pages
doi:10.1155/2008/657081

Research Article

Nonlinear Frequency Scaling Algorithm for High Squint Spotlight SAR Data Processing

Lihua Jin and Xingzhao Liu

Department of Electronic Engineering, School of Electronic, Information, and Electrical Engineering, Shanghai Jiao Tong University, 1-411 SEIEE Buildings, 800 Dongchuan Road, Shanghai 200240, China

Correspondence should be addressed to Xingzhao Liu, lxzsjtu@sina.com

Received 1 August 2007; Revised 27 December 2007; Accepted 12 February 2008

Recommended by A. Enis Çetin

This paper presents a new approach for the squint-mode spotlight SAR imaging. Like the frequency scaling algorithm, this method starts with the received signal dechirped in range. According to the geometry for the squint mode, the reference range of the dechirping function is defined as the range between the scene center and the synthetic aperture center. In our work, the residual video phase is compensated firstly to facilitate the following processing. Then the range-cell migration with a high-order range-azimuth coupling form is processed by a nonlinear frequency scaling operation, which is different from the original frequency scaling one. Due to these improvements, the algorithm can be used to process high squint SAR data with a wide swath and a high resolution. In addition, some simulation results are given at the end of this paper to demonstrate the validity of the proposed method.

1. INTRODUCTION

Spotlight synthetic aperture radar (SAR) often operates in the squint mode. Several algorithms can be used for the squint mode spotlight SAR processing, that is, the polar format algorithm (PFA) [1], the range migration algorithm (RMA) [2], the chirp scaling (CS) algorithm [3], and the frequency scaling (FS) algorithm [4], the former three of which have been comprehensively discussed in [5]. The PFA limits the quality of the final image because of polar-to-rectangular interpolation and has a higher computational burden due to two interpolations compared to the RMA technique with one interpolation [5]. The RMA is supposed to be squint angle independent. However, the interpolation degrades the image at the edges for high squint angle. Moreover, the spectrum in the range wave number direction after the Stolt mapping requires expansion and thus increases the computational load. Modified Stolt mapping methods [6, 7] introduced a change of the variable range wave number to overcome these problems.

The algorithms of CS and FS are more attractive because they avoid interpolation and the computing burden is reduced greatly. In the former algorithm, the range cell migration is approximately written as a polynomial, and is accurately corrected except the range-dependent secondary range correction (SRC) error. However, with increasing the squint angle, the error becomes significant and degrades the image. In the latter algorithm, which is presented specially for spotlight SAR data processing, the dechirped signal has been applied to reduce the sampling frequency in range. When processing high squint spotlight SAR data, the FS algorithm also suffers the trouble caused by the SRC error. Based on the CS algorithm, a nonlinear chirp scaling (NCS) algorithm [8] has been proposed to deal with the squint mode strip-map SAR imaging, in which the CS technique is extended to the cubic order to achieve the effect of the range-dependent filtering required in the SRC.

In this paper, a nonlinear frequency scaling method is presented. Inspired by the NCS algorithm, the FS operation has been extended to the cubic order to perform a more accurate SRC. Before the nonlinear frequency scaling operation, the dechirping function for the squint mode is defined, and the residual video phase is compensated to remove the side effect caused by the dechirping operation. Some simulation results for an X-band airborne spotlight SAR in the squint mode are given to demonstrate the validity of the proposed

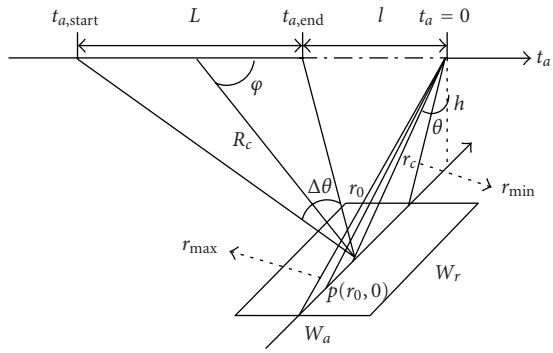

Figure 1: Squint-mode spotlight SAR geometry.

algorithm. The detailed description of the algorithm is given in Section 2, the simulation results are presented in Section 3, and the conclusion appears in Section 4.

2. ALGORITHM DESCRIPTION

2.1. Dechirping function and signal model

A simple geometry of airborne squint mode spotlight SAR is shown in Figure 1, where h is the flight altitude, θ is the angle of view, r_c is the distance from the center of the scene to the flight line, $r_{\min}$ and $r_{\max}$ are the minimum and maximum distance from the scene to the flight line, and R_c is the distance between the scene center and the synthetic aperture center. The platform moves with velocity v along a straight line, and the radar beam is steered to spotlight the scene center. The squint angle φ is defined as the angle between the view axis of the radar at the synthetic aperture center and the broadside direction.

At a certain azimuth time t_a, the slant range $R(t_a; r_0)$ between the radar sensor and a point target at position $(r_0, 0)$ can be expressed as

$$R(t_a; r_0) = \left[r_0^2 + (vt_a)^2\right]^{1/2}. \tag{1}$$

For short, $R(t_a; r_0)$ is written as $R(t_a)$ in the following text. The received chirp signal from the target is

$$\begin{aligned} s(t_a, t_e; r_0) = {} & C \cdot \text{rect}\left[\frac{t_e - 2R(t_a)/c}{T_p}\right] \\ & \times \text{rect}\left[\frac{t_a - (t_{a,\text{start}} + t_{a,\text{end}})/2}{T_{\text{spot}}}\right] \\ & \times \exp\left[-j\frac{4\pi R(t_a)}{\lambda}\right] \\ & \times \exp\left\{j\pi k_e\left[t_e - \frac{2R(t_a)}{c}\right]^2\right\}, \end{aligned} \tag{2}$$

where C is constant term, t_e is fast time, λ is the radar wavelength, k_e is the chirp rate, and c is the speed of light. T_p and T_{spot} are the pulse width and the synthetic aperture time, respectively, $t_{a,\text{start}}$ and $t_{a,\text{end}}$ are the start and the end of t_a, respectively.

In this paper, a dechirping operation is performed at the receiver. The dechirping function is defined as

$$H_{\text{Dechirp}} = \exp\left[-j\pi k_e\left(t_e - \frac{2R_c}{c}\right)^2\right], \tag{3}$$

where the reference range is chosen as R_c which is presented by the solid line in Figure 1. The dechirped signal can be described as

$$\begin{aligned} s_{\text{dechirp}}(t_a, t_e; r_0) = {} & C \cdot \text{rect}\left[\frac{t_e - 2R(t_a)/c}{T_p}\right] \\ & \times \text{rect}\left[\frac{t_a - (t_{a,\text{start}} + t_{a,\text{end}})/2}{T_{\text{spot}}}\right] \\ & \times \exp\left[-j\frac{4\pi}{\lambda}R(t_a)\right] \\ & \times \exp\left\{-j\frac{4\pi k_e}{c}[R(t_a) - R_c]\left(t_e - \frac{2R_c}{c}\right)\right\} \\ & \times \exp\left\{j\frac{4\pi k_e}{c^2}[R(t_a) - R_c]^2\right\}. \end{aligned} \tag{4}$$

According to the appendix of [4], the range Doppler domain signal after the dechirping and the azimuth Fourier transform (FT) is described as

$$\begin{aligned} & S_0(f_a, t_e; r_0) \\ & = C \cdot \left\{\text{rect}\left[\frac{t_e - 2R_c/c}{T_p}\right] \exp\left[j\frac{4\pi k_e}{c}R_c\left(t_e - \frac{2R_c}{c}\right)\right]\right. \\ & \qquad \left. \times \exp\left[-j\frac{4\pi r_0}{\lambda}\sqrt{\left[1 + \frac{\lambda k_e}{c}\left(t_e - \frac{2R_c}{c}\right)\right]^2 - \left(\frac{\lambda f_a}{2v}\right)^2}\right]\right\} \\ & \quad * \exp\left(-j\pi k_e t_e^2\right), \end{aligned} \tag{5}$$

where f_a denotes the azimuth frequency, and $*$ is the convolution operation. For the squint mode in Figure 1, the center of fast time t_e becomes $2R_c/c$, and thus

$$\left|\frac{\lambda k_e}{c}\left(t_e - \frac{2R_c}{c}\right)\right| \le \left|\frac{\lambda k_e}{c}\frac{T_p}{2}\right| = \frac{B}{2f_c} \ll 1, \tag{6}$$

where B is the bandwidth of the transmitted signal, and f_c is the carrier frequency. Therefore, the definition of the dechirping function makes the phase error small enough when the phase of the signal is expanded into the Taylor series in the range-Doppler domain.

2.2. Preprocessing residual video phase compensation

In (5), the phase of the last exponential term is called the residual video phase (RVP), which is a side effect of the dechirping. The RVP term can be removed completely from the radar signal in a preprocessing operation.

First, the dechirped signal is transformed into the range frequency domain, according to (C.8) and (C.9) in the appendix of [5], where the constant term C is omitted:

$$\begin{aligned} S_1(t_a, f_e; r_0) = {} & \exp\left[-j\frac{4\pi}{\lambda}R(t_a)\right] \\ & \times \exp\left\{ -j\frac{4\pi k_e}{c^2}[R(t_a) - R_c]^2\right\} \\ & \times \exp\left[-j\frac{4\pi R(t_a)}{c}f_e\right] \\ & \times T_p \mathrm{sinc}\left\{\pi T_p\left[f_e + \frac{2k_e}{c}(R(t_a) - R_c)\right]\right\}, \end{aligned} \tag{7}$$

where f_e is the range frequency. Since $F = f_e + (2k_e/c)[R(t_a) - R_c]$ and $\exp(-j\pi/k_e \cdot F^2) \approx 1$ when $-1/T_p < F < 1/T_p$, therefore (7) can be simplified as

$$\begin{aligned} S_2(t_a, f_e; r_0) = {} & T_p \mathrm{sinc}\,(\pi T_p F)\exp\left[-j\frac{4\pi}{\lambda}R(t_a)\right] \\ & \times \exp\left(-j\frac{4\pi R_c}{c}f_e\right)\exp\left(j\frac{\pi}{k_e}f_e^2\right). \end{aligned} \tag{8}$$

The last exponential term $\exp(j\pi/k_e \cdot f_e^2)$ in the frequency domain expression of (8) corresponds to the RVP term in the time domain expression of (5). Multiplied by a phase compensation function, the RVP term can be removed in the range frequency domain. In the domain of fast time and slow time, the output is

$$\begin{aligned} S_3(t_a, t_e; r_0) = {} & \mathrm{rect}\left[\frac{t_e - 2R_c/c}{T_p}\right]\exp\left[-j\frac{4\pi}{\lambda}R(t_a)\right] \\ & \times \exp\left\{ -j\frac{4\pi k_e}{c}[R(t_a) - R_c]\left(t_e - \frac{2R_c}{c}\right)\right\}. \end{aligned} \tag{9}$$

2.3. Nonlinear frequency scaling algorithm

Transforming (9) by the principle of stationary phase [9] for the azimuth Fourier transformation, we can obtain the range-Doppler domain expression similar to (5), that is,

$$\begin{aligned} & S_4(f_a, t_e; r_0) \\ & = \mathrm{rect}\left[\frac{t_e - 2R_c/c}{T_p}\right]\exp\left[j\frac{4\pi k_e}{c}R_c\left(t_e - \frac{2R_c}{c}\right)\right] \\ & \quad \times \exp\left[-j\frac{4\pi r_0}{\lambda}\sqrt{\left[1 + \frac{\lambda k_e}{c}\left(t_e - \frac{2R_c}{c}\right)\right]^2 - \left(\frac{\lambda f_a}{2v}\right)^2}\right]. \end{aligned} \tag{10}$$

After a Taylor series expansion of the square root expression in (10), the signal is written as

$$\begin{aligned} S_4'(f_a, t_e; r_0) = {} & \mathrm{rect}[\cdot]\exp\left(-j\frac{4\pi r_0\beta}{\lambda}\right) \\ & \times \exp\left[-j\frac{4\pi k_e}{c}\left(\frac{r_0}{\beta} - R_c\right)\left(t_e - \frac{2R_c}{c}\right)\right] \\ & \times \exp\left[-j\frac{\pi}{K_m}\left(t_e - \frac{2R_c}{c}\right)^2\right] \\ & \times \exp\left[j\phi_3\left(t_e - \frac{2R_c}{c}\right)^3\right]. \end{aligned} \tag{11}$$

Generally, the quartic and the higher-order errors can be neglected even in the case of a large squint angle. In (11),

$$\begin{aligned} \beta(f_a) &= \sqrt{1 - \left[\frac{\lambda(f_a + f_{\mathrm{dc}})}{2v}\right]^2}, \\ K_m &= \frac{c^2\beta^3}{2\lambda k_e^2(\beta^2 - 1)r_0} = K_{m\mathrm{ref}} + K_s \cdot \Delta f, \\ K_{m\mathrm{ref}} &= \frac{c^2\beta^3}{2\lambda k_e^2(\beta^2 - 1)r_c}, \\ K_s &= \frac{c^3\beta^4}{4\lambda k_e^3(\beta^2 - 1)r_c^2}, \\ \Delta f &= -\frac{2k_e}{c\beta}(r_0 - r_c), \\ \phi_3 &= \frac{2\pi\lambda^2 k_e^3 r_0}{c^3}\frac{\beta^2 - 1}{\beta^5}. \end{aligned} \tag{12}$$

In (12), f_{dc} is Doppler centroid, K_m is written as the sum of a constant term and a linear term. In [4], the original FS operation scales the range frequency by $1/\beta$, that is, the main part of the phase in (11) is scaled as

$$-\frac{4\pi k_e}{c\beta}(r_0 - R_c\beta)\left(t_e\beta - \frac{2R_c}{c}\right) - \frac{\pi}{K_m}\left(t_e\beta - \frac{2R_c}{c}\right)^2 + \cdots. \tag{13}$$

The secondary range compression and the bulk range shift are performed by

$$+\frac{4\pi k_e}{c\beta}(r_c - R_c\beta)\left(t_e\beta - \frac{2R_c}{c}\right) + \frac{\pi}{K_{m\mathrm{ref}}}\left(t_e\beta - \frac{2R_c}{c}\right)^2 - \cdots. \tag{14}$$

Obviously, the phase compensation of the FS algorithm is completed only for the second exponential term in (11). The quadratic and the cubic exponential terms in (11) are defined to be $\mathrm{src}(f_a, t_e; r_0)$ which is referred to as the secondary range compression term in [4], and are compensated by $\mathrm{src}(r_{\mathrm{ref}})^*$ in the FS algorithm, where r_c is chosen as the reference range r_{ref}. However, in the case of a large squint angle and a large scene, the error from approximation $r_0 \approx r_{\mathrm{ref}}$ ($K_m \approx K_{m\mathrm{ref}}$) cannot be neglected any longer, and the phase error caused by the incompletely matched $\mathrm{src}(r_{\mathrm{ref}})^*$ distorts the image severely.

The quadratic and cubic phases $\varphi_2 = -(\pi/K_m)(t_e - 2R_c/c)^2$, $\varphi_3 = \phi_3(t_e - 2R_c/c)^3$ are the function of azimuth frequency f_a, range time t_e, and the target range. The

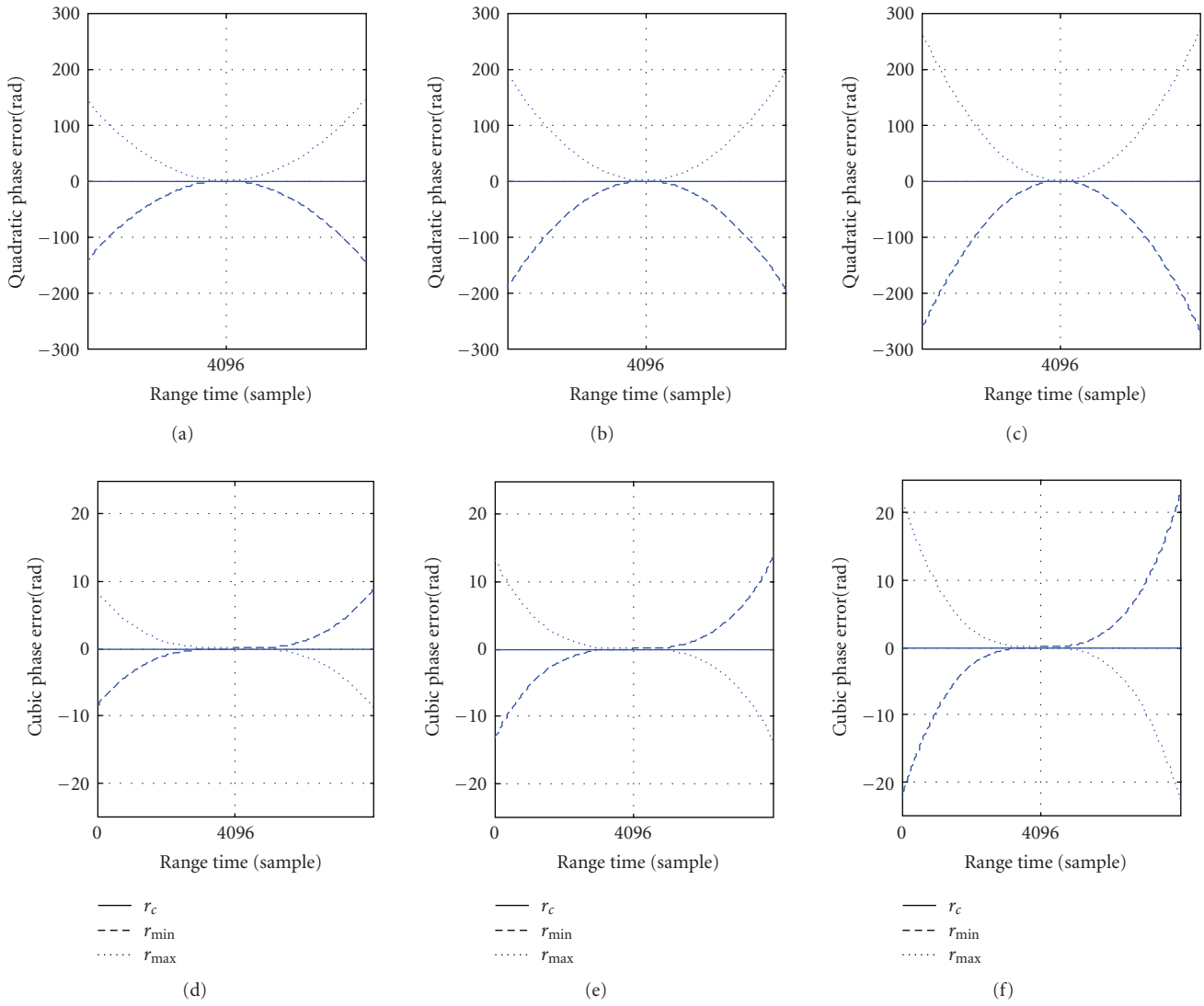

FIGURE 2: (a), (b), and (c) present the quadratic phase error $\varphi_2 - \varphi_2(r_c)$ in the case of $\beta(-\text{PRF}/2) = 0.5394$, $\beta(0) = 0.5$, and $\beta(\text{PRF}/2) = 0.4559$, respectively. (d), (e), and (f) present the cubic phase error $\varphi_3 - \varphi_3(r_c)$ at three different β values 0.5394, 0.5, and 0.4559.

following simulation result presents the quadratic and cubic phase error for 60 degree squint angle with particular parameters listed in Section 3.

The quadratic phase error shown in Figure 2 is too large to make the image focused. Therefore, the quadratic phase error has to be compensated. However, the cubic phase error is acceptable if compared with the quadratic phase error.

A nonlinear method [8] has been used to solve this problem caused by the approximation error, where the coefficient of the quadratic term is also scaled to be range independent. In the proposed algorithm, the main part of phase in (11) after the nonlinear FS can be written as

$$-\frac{4\pi k_e}{c\beta}(r_0 - R_c\beta)\left(t_e\beta - \frac{2R_c}{c}\right) - \frac{\pi}{K_{m\text{ref}}\beta}\left(t_e\beta - \frac{2R_c}{c}\right)^2 + \cdots. \tag{15}$$

Though (11) is not a strict chirp signal, if the cubic term is small enough, it is possible to apply the principle of stationary phase to obtain its FT. The fundamental FT pair in the nonlinear operation can be described as

$$\exp\left(-j\frac{\pi}{k}t^2\right)\exp\left(-j\frac{2\pi}{3}yt^3\right) \Longleftrightarrow \exp\left(j\pi k f^2\right)\exp\left(j\frac{2\pi}{3}yk^3f^3\right), \tag{16}$$

where the coefficient y should satisfy $|y| \ll 1/|4k^2 f|$. The derivation is given in Appendix A.

2.4. Phase compensation functions

The block diagram of the nonlinear FS algorithm is shown in Figure 3. The signal at the stage of the dashed line box below in Figure 3 corresponds to (11). In order to accurately compensate the quadratic term and minimize the errors

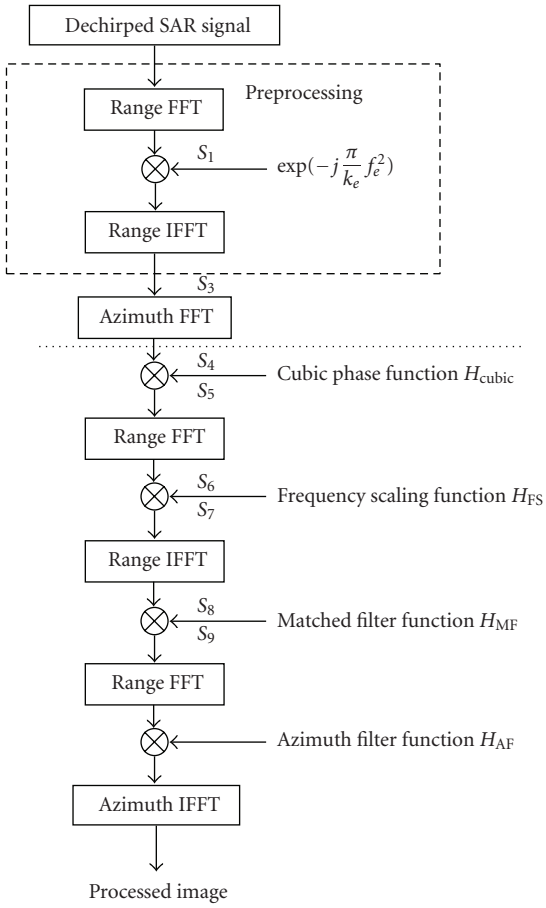

Figure 3: Block diagram of the nonlinear frequency scaling algorithm.

from higher-order terms, a small-phase filter function is multiplied before the FS operation, that is,

$$H_{\text{cubic}} = \exp\left\{ -j\frac{2\pi}{3}\left[Y_m + \frac{3}{2\pi}\phi(r_{\text{ref}})\right]\left(t_e - \frac{2R_c}{c}\right)^3\right\}, \tag{17}$$

where $Y_m = K_s(1/\beta - 0.5)/K_{m\text{ref}}^3(1/\beta - 1)$. The derivation of Y_m is given in Appendix B. The output of the cubic filter is approximately written as

$$\begin{aligned} S_5(f_a, t_e; r_0) &= S_4'(f_a, t_e; r_0)\cdot H_{\text{cubic}} \\ &= \text{rect}[\cdot]\exp\left(-j\frac{4\pi r_0\beta}{\lambda}\right) \\ &\quad\times\exp\left[-j\frac{4\pi k_e}{c}\left(\frac{r_0}{\beta} - R_c\right)\left(t_e - \frac{2R_c}{c}\right)\right] \\ &\quad\times\exp\left[-j\frac{\pi}{K_m}\left(t_e - \frac{2R_c}{c}\right)^2\right] \\ &\quad\times\exp\left[-j\frac{2\pi}{3}Y_m\left(t_e - \frac{2R_c}{c}\right)^3\right]. \end{aligned} \tag{18}$$

According to (16), we can write the expression after the range FT as

$$\begin{aligned} S_6(f_a, f_e; r_0) &= \exp\left(-j\frac{4\pi r_0}{\lambda}\beta\right) \\ &\quad\times\exp\left[-j\frac{4\pi R_c}{c}(f_e - f_d)\right] \\ &\quad\times\exp\left[j\pi K_m(f_e - f_d)^2\right] \\ &\quad\times\exp\left[j\frac{2\pi}{3}Y_m K_m^3(f_e - f_d)^3\right], \end{aligned} \tag{19}$$

where

$$\begin{aligned} f_d &= -\frac{2k_e}{c}\left(\frac{r_0}{\beta} - R_c\right) = \frac{2k_e}{c}\left(R_c - \frac{r_c}{\beta}\right) + \frac{2k_e}{c\beta}(r_c - r_0) \\ &= f_{\text{ref}} + \Delta f, \quad f_{\text{ref}} = \frac{2k_e}{c}\left(R_c - \frac{r_c}{\beta}\right), \end{aligned} \tag{20}$$

where f_d is the counterpart of the scatterer trajectory τ_d mentioned in the NCS algorithm [8]. The frequency f_d is moved to the desired trajectory $f_s = f_{\text{ref}} + \beta\cdot\Delta f$ after the nonlinear FS operation, and thus the range migration can be corrected.

The frequency scaling function is extended to the cubic order such that the coefficient of the quadratic term is scaled as a range-independent one, that is,

$$\begin{aligned} H_{\text{FS}} &= \exp\left[j\frac{4\pi R_c}{c}\left(1 - \frac{1}{\beta}\right)(f_e - f_{\text{ref}})\right] \\ &\quad\times\exp\left[j\pi q_2(f_e - f_{\text{ref}})^2\right] \\ &\quad\times\exp\left[j\frac{2\pi}{3}q_3(f_e - f_{\text{ref}})^3\right], \end{aligned} \tag{21}$$

where $q_2 = K_{m\text{ref}}(1/\beta - 1), q_3 = K_s(1/\beta - 1)/2$.

Multiplied by H_{FS}, the signal becomes as follows:

$$\begin{aligned} S_7(f_a, f_e; r_0) &= S_6(f_a, f_e; r_0)\cdot H_{\text{FS}} \\ &= \exp\left(-j\frac{4\pi r_0}{\lambda}\beta\right)\exp\left[-j\frac{4\pi R_c}{c\beta}(f_e - f_s)\right] \\ &\quad\times\exp\left[j\pi\frac{K_{\text{ref}}}{\beta}(f_e - f_s)^2\right] \\ &\quad\times\exp\left[j\frac{2\pi}{3}\frac{K_s}{2\beta(1-\beta)}(f_e - f_s)^3\right]\exp(j\phi_\Delta). \end{aligned} \tag{22}$$

The derivation of (22) and the definition of ϕ_Δ are also given in Appendix B. According to (16), the signal after the inverse FT in range can be expressed as

$$\begin{aligned} S_8(f_a, t_e; r_0) &= \exp\left(-j\frac{4\pi r_0}{\lambda}\beta\right)\exp\left[j2\pi f_s\left(t_e - \frac{2R_c}{c\beta}\right)\right] \\ &\quad\times\exp\left[-j\frac{\pi\beta}{K_{m\text{ref}}}\left(t_e - \frac{2R_c}{c\beta}\right)^2\right] \\ &\quad\times\exp\left[-j\frac{\pi}{3}\frac{K_s\beta^2}{K_{m\text{ref}}^3(1-\beta)}\left(t_e - \frac{2R_c}{c\beta}\right)^3\right] \\ &\quad\times\exp(j\phi_\Delta). \end{aligned} \tag{23}$$

Table 1: System parameters for an airborne X-band SAR.

Wavelength	Altitude h	Slant range R_c	Velocity v	Ground resolution	Scene size
0.03 m	4 Km	60 Km	200 m/s	1 m × 1 m	1 Km × 1 Km

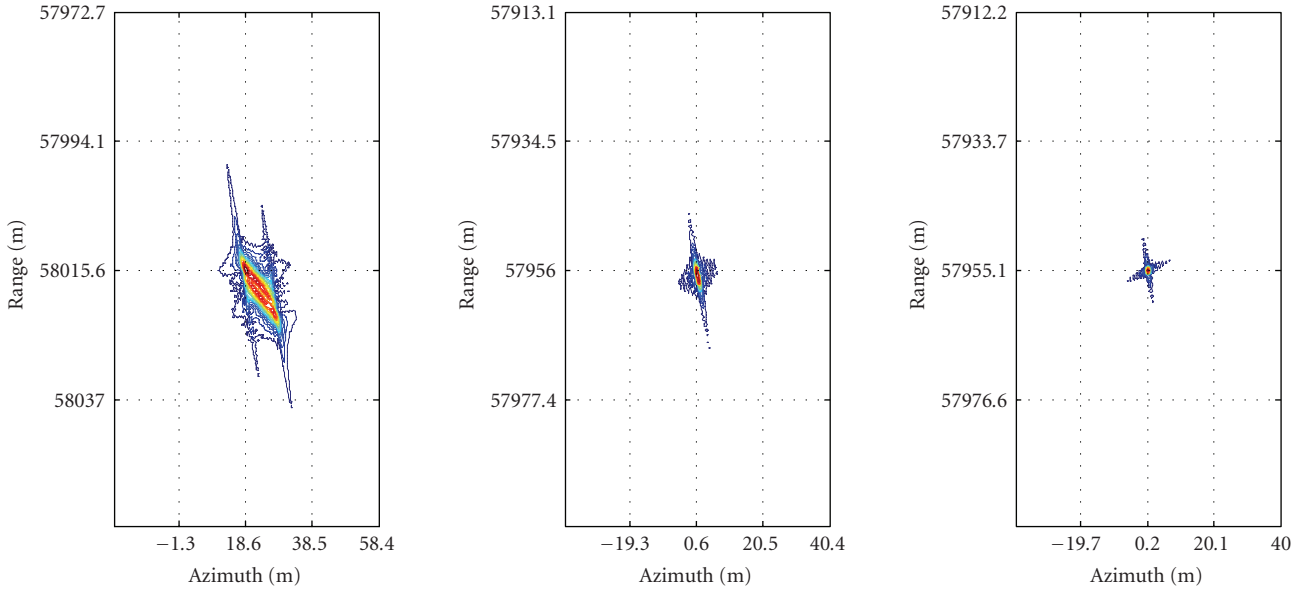

Figure 4: Contour plots of point target by different algorithms (squint angle $\varphi = 15^\circ$). (a) Processed by the FS algorithm [4]. (b) Processed by the FS algorithm with the dechirping function given in this paper. (c) Processed by the nonlinear FS algorithm.

After the multiplication by the frequency scaling function H_{FS} and the inverse FT in range, the secondary range compression and the bulk range cell migration correction (RCMC) can be performed using the range-matched filter function. The range-matched filter function is given by

$$H_{\mathrm{MF}} = \exp\left[-j2\pi f_{\mathrm{ref}}\left(t_e - \frac{2R_c}{c\beta}\right)\right] \times \exp\left[j\frac{\pi\beta}{K_{m\mathrm{ref}}}\left(t_e - \frac{2R_c}{c\beta}\right)^2\right] \times \exp\left[j\frac{\pi K_s\beta^2}{3K_{m\mathrm{ref}}^3(1-\beta)}\left(t_e - \frac{2R_c}{c\beta}\right)^3\right]. \quad (24)$$

After the range-matched filtering and the range FT, the signal is focused in range, that is,

$$S_9(f_a, f_e; r_0) = \exp\left(-j\frac{4\pi r_0}{\lambda}\beta\right)\mathrm{sinc}\left[f_e + \frac{2k_e}{c}(r_0 - r_c)\right] \times \exp\left(-j2\pi\frac{2R_c}{c\beta}f_e\right)\exp(j\phi_\Delta). \quad (25)$$

Finally, a focused image can be obtained by the azimuth filtering and the azimuth inverse FT. The azimuth filter function is given as follows:

$$H_{\mathrm{AF}} = \exp\left[-j\frac{4\pi r_0}{\lambda}(1-\beta)\right]\exp(-j\phi_\Delta)\exp\left(j2\pi\frac{2R_c}{c\beta}f_e\right). \quad (26)$$

Shifting the range spectrum to make $f_{\mathrm{ref}} = 0$ before the frequency scaling operation will simplify the expressions of H_{FS}, H_{MF}, and H_{AF}.

3. SIMULATION RESULTS

In order to evaluate the proposed algorithm, some simulations for an airborne spotlight SAR in the squint mode have been performed. The system parameters are given in Table 1.

First, the results obtained by using the FS algorithm [4], the FS algorithm with the dechirping function given in this paper and the proposed algorithm, have been compared. The squint angle is defined as 15 degree. The echo of a point target at the center of the scene is simulated and the contour plots by the three algorithms are shown in Figure 4. From Figure 4, the contour of point target by the FS algorithm [4] is defocused so severe that the target cannot be identified; the image by the FS algorithm with the dechirping function given in this paper is acceptable, however, its main lobe is broadened and represents a small position shift; as expectation the image processed by the proposed algorithm shows excellent focus performance and the range and azimuth peak position all agree with the theoretical values.

Another simulation under the same system parameters with the squint angle $\varphi = 60^\circ$ is implemented. The distance from the center of the scene to the flight path r_c is 30 km, the synthetic aperture L is 1800 m, the signal bandwidth is

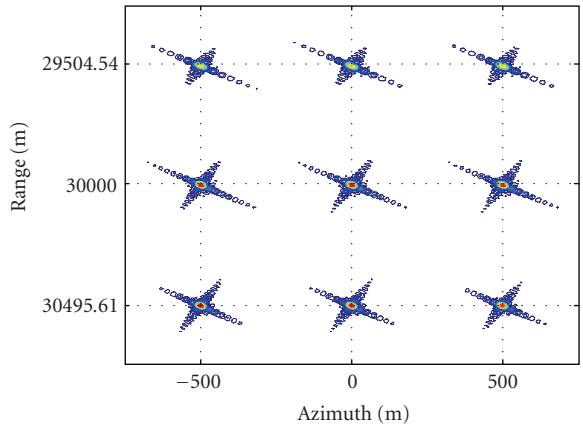

Figure 5: Contour plot of targets (squint angle $\varphi = 60^\circ$), where the image of each target has been zoomed and then pasted back into original figure according to its location.

151.35 MHz, the pulse width is 20 microseconds, and the PRF is 640 Hz. Nine typical point targets are arranged in the scene. Their range coordinates are $r_{\max}$, r_c, and $r_{\min}$, and their azimuth coordinates are −500 m, 0, and 500 m, respectively. The Doppler centroid is not zero, and thus the azimuth spectrum should be shifted before being transformed into the range-Doppler domain. The contour plot of the nine targets is shown in Figure 5. The simulation results show that the nonlinear frequency scaling method is also effective even in the squint angle up to 60 degree, which can obtain images with high quality even at the edges of a large scene.

4. CONCLUSION

In this paper, we present a squint mode spotlight SAR processing scheme. With the phase error correction, a complete processing flow for the squint mode spotlight SAR is proposed. First, a dechirping function for the squint mode is given. Then a preprocessing step is introduced to remove the RVP. Finally, the nonlinear approach and the frequency scaling operation are combined to minimize the approximation error of the SRC. The simulation results show that the proposed algorithm is quite effective in the case of high squint angle and large scene. In addition, only the FT and multiplication operations are required in this algorithm.

APPENDICES

A. DERIVATION OF FOURIER TRANSFORMS PAIR FOR A NONLINEAR CHIRP SIGNAL

Consider a signal

$$x(t) = \exp\left(-j\frac{\pi}{k}t^2\right)\exp\left(-j\frac{2\pi}{3}yt^3\right), \tag{A.1}$$

we can use the principle of stationary phase to obtain its FT. The integral phase can be written as follows:

$$\phi(t) = -\frac{\pi}{k}t^2 - \frac{2\pi}{3}yt^3 - 2\pi ft. \tag{A.2}$$

According to the principle, the stationary points that make the most contributions satisfy the following:

$$\frac{d}{dt}\phi(t) = -\frac{2\pi}{k}t - 2\pi yt^2 - 2\pi f = 0. \tag{A.3}$$

The solution to this equation is

$$t = \frac{-1 \pm \sqrt{1 - 4fk^2y}}{2ky}, \quad \text{when } |y| \ll \frac{1}{|4k^2f|},\ t \approx -kf. \tag{A.4}$$

Substituting the solution into the integral phase expression, we can obtain the phase of the FT, that is,

$$\phi(f) = \pi kf^2 + \frac{2\pi}{3}yk^3f^3. \tag{A.5}$$

As a result, we can obtain the FT pair in (16).

B. DERIVATION OF THE NONLINEAR FREQUENCY SCALING FUNCTION

In this section, the derivation of variables q_2, q_3, Y_m, ϕ_Δ is presented. Here, (19) and (21) are rewritten as (B.1) and (B.2) as follows:

$$\begin{aligned} S_6(f_a, f_e; r_0) = {} & \exp\left(-j\frac{4\pi r_0}{\lambda}\beta\right)\exp\left[-j\frac{4\pi R_c}{c}(f_e - f_d)\right] \\ & \times \exp\left[j\pi K_m(f_e - f_d)^2\right] \\ & \times \exp\left[j\frac{2\pi}{3}Y_mK_m^3(f_e - f_d)^3\right], \end{aligned} \tag{B.1}$$

$$\begin{aligned} H_{\mathrm{FS}} = {} & \exp\left[j\frac{4\pi R_c}{c}\left(1 - \frac{1}{\beta}\right)(f_e - f_{\mathrm{ref}})\right] \\ & \times \exp\left[j\pi q_2(f_e - f_{\mathrm{ref}})^2\right] \\ & \times \exp\left[j\frac{2\pi}{3}q_3(f_e - f_{\mathrm{ref}})^3\right]. \end{aligned} \tag{B.2}$$

Multiplied (B.1) by (B.2), that is, ${S_6}^* H_{\mathrm{FS}}$, the quadratic and the cubic terms of the phase expression can be written as a polynomial of $f_e - f_s$, where constant π is neglected:

$$\begin{aligned} & K_m(f_e - f_d)^2 + \frac{2}{3}Y_mK_m^3(f_e - f_d)^3 + q_2(f_e - f_{\mathrm{ref}})^2 + \frac{2}{3}q_3(f_e - f_{\mathrm{ref}})^3 \\ & \quad = C_3(f_e - f_s)^3 + C_2(f_e - f_s)^2 + C_1(f_e - f_s) + C_0, \end{aligned} \tag{B.3}$$

where the relationships $f_d = f_{\mathrm{ref}} + \Delta f$, $f_s = f_{\mathrm{ref}} + \beta \cdot \Delta f$ have been applied and the polynomial coefficients of $f_e - f_s$ can be calculated as

$$\begin{aligned} C_3 &= \frac{2}{3}(Y_mK_m^3 + q_3), \\ C_2 &= 2(Y_mK_m^3 + q_3)\beta\Delta f + (K_m + q_2 - 2Y_mK_m^3\Delta f), \\ C_1 &= 2(Y_mK_m^3 + q_3)\beta^2\Delta f^2 + 2(K_m + q_2 - 2Y_mK_m^3\Delta f)\beta\Delta f \\ &\quad + (2Y_mK_m^3\Delta f^2 - 2K_m\Delta f). \end{aligned} \tag{B.4}$$

In (B.4), unknown variables q_2, q_3, and Y_m are used to make that C_1, C_2, and C_3 are independent of Δf. Expanding C_1, C_2, and C_3 into polynomials of $\Delta f = (2k_e/c\beta)(r_c - r_0)$ and substituting the expression of $K_m = K_{mref} + K_s \cdot \Delta f$, therefore, the coefficient of the cubic term is as follows:

$$C_3 = \frac{2}{3}\left(Y_m K_{mref}^3 + q_3\right) + 2Y_m K_{mref}^2 K_s \Delta f + 2Y_m K_{mref} K_s^2 \Delta f^2 + \frac{2}{3} Y_m K_s^3 \Delta f^3, \tag{B.5}$$

and the coefficient of the quadratic term

$$C_2 = K_{mref} + q_2 + \left[K_s + 2q_3\beta + 2Y_m K_{mref}^3 (\beta - 1)\right]\Delta f + 6Y_m K_{mref}^2 K_s (\beta - 1)\Delta f^2 + \cdots, \tag{B.6}$$

and the coefficient of the linear term

$$C_1 = \left[2K_{mref}(\beta - 1) + 2q_2\beta\right]\Delta f + \left[2Y_m K_{mref}^3 (\beta - 1)^2 + 2q_3\beta^2 + 2K_s(\beta - 1)\right]\Delta f^2 + 6Y_m K_{mref}^2 K_s (\beta - 1)^2 \Delta f^3 + \cdots. \tag{B.7}$$

In order to compensate src term exactly, the coefficients of Δf in (B.5), (B.6), and (B.7) are preferred to be zero. However, the case of $Y_m = 0$ is meaningless, thus, the following equations hold:

$$\begin{aligned} K_s + 2q_3\beta + 2Y_m K_{mref}^3 (\beta - 1) &= 0, \\ 2K_{mref}(\beta - 1) + 2q_2\beta &= 0, \\ 2Y_m K_{mref}^3 (\beta - 1)^2 + 2q_3\beta^2 + 2K_s(\beta - 1) &= 0. \end{aligned} \tag{B.8}$$

Solving the linear equations, we obtain

$$q_2 = K_{mref}\left(\frac{1}{\beta - 1}\right), \qquad q_3 = \frac{K_s(1/\beta - 1)}{2}, \qquad Y_m = \frac{K_s(1/\beta - 0.5)}{K_{mref}^3 (1/\beta - 1)}. \tag{B.9}$$

By ignoring higher-order terms of Δf in the coefficients of $f_e - f_s$, (B.3) is approximated as follows:

$$\frac{2}{3}\left(Y_m K_{mref}^3 + q_3\right)\left(f_e - f_s\right)^3 + \left(K_{mref} + q_2\right)\left(f_e - f_s\right)^2 + \cdots = A\left(f_e - f_s\right)^2 + \frac{2}{3} BA^3 \left(f_e - f_s\right)^3 + \phi_\Delta, \tag{B.10}$$

where

$$\begin{aligned} A &= \frac{1}{\beta} K_{mref}, \\ BA^3 &= \frac{K_s}{2\beta(1-\beta)}, \\ \phi_\Delta &= \left[-\frac{2}{3} Y_m K_s^3\right]\Delta f^6 + \left[-2Y_m K_{mref} K_s^2 - 2Y_m K_s^3 f_{ref}\right]\Delta f^5 \\ &\quad + \left[-2Y_m K_{mref}^2 K_s^2 - 6Y_m K_{mref} K_s^2 f_{ref} - 2Y_m K_s^3 f_{ref}^2\right]\Delta f^4 \\ &\quad + \left[\frac{K_s}{3}(1 - \beta) - 6Y_m K_{mref}^2 K_s f_{ref} - 6Y_m K_{mref} K_s^2 f_{ref}^2 - \frac{2}{3} Y_m K_s^3 f_{ref}^3\right]\Delta f^3 \\ &\quad + \left[K_{mref}(1 - \beta) - 6Y_m K_{mref}^2 K_s f_{ref}^2 - 2Y_m K_{mref} K_s^2 f_{ref}^3\right]\Delta f^2 + \left[-2Y_m K_{mref}^2 K_s f_{ref}\right]\Delta f. \end{aligned} \tag{B.11}$$

REFERENCES

[1] M. Soumekh, *Synthetic Aperture Radar Signal Processing with MATLAB Algorithms*, John Wiley & Sons, New York, NY, USA, 1999.

[2] C. Cafforio, C. Prati, and F. Rocca, "SAR data focusing using seismic migration techniques," *IEEE Transactions on Aerospace and Electronic Systems*, vol. 27, no. 2, pp. 194–207, 1991.

[3] R. K. Raney, H. Runge, R. Bamler, I. G. Cumming, and F. H. Wong, "Precision SAR processing using chirp scaling," *IEEE Transactions on Geoscience and Remote Sensing*, vol. 32, no. 4, pp. 786–799, 1994.

[4] J. Mittermayer, A. Moreira, and O. Loffeld, "Spotlight SAR data processing using the frequency scaling algorithm," *IEEE Transactions on Geoscience and Remote Sensing*, vol. 37, no. 5, part 1, pp. 2198–2214, 1999.

[5] G. Carrara, R. S. Goodman, and R. M. Majewski, *Spotlight Synthetic Aperture Radar*, Artech House, Norwood, Mass, USA, 1995.

[6] A. Reigber, E. Alivizatos, A. Potsis, and A. Moreira, "Extended wavenumber-domain synthetic aperture radar focusing with integrated motion compensation," *IEE Proceedings: Radar, Sonar and Navigation*, vol. 153, no. 3, pp. 301–310, 2006.

[7] M. Vandewal, R. Speck, and H. Süß, "Efficient and precise processing for squinted spotlight SAR through a modified stolt mapping," *EURASIP Journal on Advances in Signal Processing*, vol. 2007, Article ID 59704, 7 pages, 2007.

[8] G. W. Davidson, I. G. Cumming, and M. R. Ito, "A chirp scaling approach for processing squint mode SAR data," *IEEE Transactions on Aerospace and Electronic Systems*, vol. 32, no. 1, pp. 121–133, 1996.

[9] J. C. Curlander and R. N. McDonough, *Synthetic Aperture Radar: Systems and Signal Processing*, John Wiley & Sons, New York, NY, USA, 1991.